Results in Physics 5 (2015) 206–221

Contents lists available at ScienceDirect

Results in Physics

journal homepage: www.journals.elsevier.com/results-in-physics

Prediction of load threshold of fibre-reinforced laminated composite panels subjected to low velocity drop-weight impact using efficient data filtering techniques

Umar Farooq *, Peter Myler

Faculty of Engineering and Advanced Sciences, University of Bolton, BL3 5AB, United Kingdom

ARTICLE INFO

Article history:
Received 26 June 2015
Accepted 29 July 2015
Available online 3 August 2015

Keywords:
Carbon fibre
Polymeric composites
Mechanical testing
Data filtering

ABSTRACT

This work is concerned with physical testing of carbon fibrous laminated composite panels with low velocity drop-weight impacts from flat and round nose impactors. Eight, sixteen, and twenty-four ply panels were considered. Non-destructive damage inspections of tested specimens were conducted to approximate impact-induced damage. Recorded data were correlated to load–time, load–deflection, and energy–time history plots to interpret impact induced damage. Data filtering techniques were also applied to the noisy data that unavoidably generate due to limitations of testing and logging systems. Built-in, statistical, and numerical filters effectively predicted load thresholds for eight and sixteen ply laminates. However, flat nose impact of twenty-four ply laminates produced clipped data that can only be de-noised involving oscillatory algorithms. Data filtering and extrapolation of such data have received rare attention in the literature that needs to be investigated. The present work demonstrated filtering and extrapolation of the clipped data using Fast Fourier Convolution algorithm to predict load thresholds. Selected results were compared to the damage zones identified with C-scan and acceptable agreements have been observed. Based on the results it is proposed that use of advanced data filtering and analysis methods to data collected by the available resources has effectively enhanced data interpretations without resorting to additional resources. The methodology could be useful for efficient and reliable data analysis and impact-induced damage prediction of similar cases' data.

1. Introduction

Carbon fibre thin laminates are being widely used as building blocks of aircraft and modern light-weight structures due to their high elastic modulus and high strength. However, their behaviour under the flat nose low velocity tool (tool box) drop impacts during part assembly, manufacturing, normal service, and maintenance operations is a major concern. Such impacts could cause barely visible internal damage. The invisible damage could severely reduce compressive strength of the impacted sub-component during future operations and might result in un-expected catastrophic failure. Extensive investigations are being carried out on various aspects of the topic in order to maintain level of quality and safety required to avoid failure. Selected and most relevant studies are referred below for further details.

Widely used drop-weight impact testing and damage measuring procedures of laminated plates are documented in (ASTM: D7136). Impact damage resistance and damage tolerance of fibre reinforced laminated composites using different approaches to assess impact induced damage are reported in [1,2]. Effect of impactor shapes and geometries were investigated in [3–5]. The damage response on multilayer plates and stacking sequences is reported in [6,7]. Mainly utilised non-destructive techniques in aircraft industry consisting of: visual inspection, ultra-sonic C-scans and Eddy-current are reported in [8,9]. The techniques produce a planar indication of the type and extent of damage to detect certain kinds of damage distribution and progression without causing any major damage to the laminate that can be re-used or further tested. Main disadvantages and limitations of using the techniques are: whole structure has to be inspected, inspection process causes interruptions in normal operations and delays, and produces two-dimensional scan plots where multi-plane delaminations are projected on a single plane [10–12]. Hence, the techniques need to be supplemented with the data analysis for impact induced damage interpretations and analyses.

* Corresponding author at: University of Bolton, Bolton BL3 5AB, United Kingdom. Tel./fax: +44 01204 903011.
E-mail addresses: adalzai3@yahoo.co.uk, uf1res@bolton.ac.uk (U. Farooq).

http://dx.doi.org/10.1016/j.rinp.2015.07.007
2211-3797/

Common difficulty in measuring data, analysis, and damage detection is the contamination of noise due to vibration of impactor, target, rig, and other apparatus at different frequencies [13].

Damage detections in impacted composite laminates using de-noising and frequency response methods are described in [14]. De-noising the impact produced data and damage detection by means of electrical potential techniques are reported in [15,16]. The studies report that the impact produced noise could amplify and distort data interpretation and analysis [17]. It has been reported that three-dimensional elasticity theory based finite element analysis combined with the low velocity impact tests could reduce the noise in [18]. Another study to reduce the difficulty with data analysis based on coupled finite element and Kalman filter is proposed in [19]. A new sigma-point (linear regression based) Kalman filter was proposed in [20] to address nonlinearities induced by inter-laminar lay-ups. The filter uses the first order Taylor series expansion and accordingly updates statistics of the structural state. Improved estimates on delamination state and parameter identification via joint Kalman linear statistical filters are reported in [21].

In addition to the traditional data filtering and time signal averaging techniques, the Fast Fourier Transforms are also being applied to filter and analyse data in material damage detection for many years [22,23]. Filtered curves were used in conjunction with the unfiltered curves to predict the threshold load [24]. Laminates of three types of lay-ups: eight, sixteen and twenty-four were tested using round and flat round nose impact profiles. Components of higher frequencies were filtered so that only harmonics of fundamental frequency level responses could be seen as reported in [25]. Experimental results have shown significant improvement in accuracy with using the FFT-Convolution techniques as signal analysis tool greatly aid in interpretation of the data [23].

Impact generated data were filtered, threshold loads were predicted, compared and correlated to the relevant C-scan identified damage zones and were found within acceptable (±12%) deviations. The results proposed that use of advanced data filters can enhance interpretation of the data recorded with the available resources and make the investigation more efficient and reliable.

2. Materials of laminated composite panels

Carbon fibre composites were developed by combining two or more engineering materials reinforced with strong material fibres to obtain a useful third material that exhibits better mechanical properties and economic values. Most of the composite materials are made by stacking several distinct layers of unidirectional lamina/ply made of the same constituent materials: matrix and fibres. The laminates used in this study were donated by industry, made of aerospace grade carbon fibre reinforced toughened epoxy infused Fibre dux 914C-833-40 embedded with satin weave fibre horn technique of every fifth ply. Stacking sequence code is $[0/45/\text{-}45/90]_{ns}$ for the symmetrical laminates where the subscript 's' stands for symmetric and 'n' varies from 1, 2, and 3 for repetition of the lay-ups. In-plane dimensions of the laminates consist of plane dimensions of 150 mm × 120 mm. Panels have average variable thickness: 2.4 (±0.02), 4.8 (±0.023), and 7.2 (±0.026) mm respectively as shown in schematic view Fig. 1.

The uniform material properties of individual layer in the laminates were assumed as given in Table 1.

3. Outline of the study

An outline of the investigation is depicted in flowchart Fig. 2. Physical tests were conducted of the panels shown in Fig. 1. Non-destructive examinations of the impacted specimens were performed. Impact produced data were analysed using built-in, statistical, numerical and fast Fourier filters. Data analysis assisted using filters to remove the low frequency impact response so that they could not dominate the high frequency signals.

4. Impact tester and drop-weight impact testing

The tests were performed analogous to the actual impact event of real materials using an instrumented drop-weight testing system, INSTRON™ Pneumatic Dynatup System 9250HV (Products, 2011) shown in Fig. 3. The drop-weight machine represents situations such as accidentally falling of drop hammer, tool (box) during fabrication or maintenance, kitchen van etc. The test system is suitable for a wide variety of applications requiring low to high impact energies using an instrumented falling weight with no energy storage device. The maximum impact energy is limited by the adjustable falling height. The target clamping fixture sandwiches laminate between two rectangular steel plates that had circular central holes for 50 mm diameters test area. Flat and round nose shape steel impactors were used in the study. The flat type impact is regarded as common danger in aerospace industry hence the nose shape was fabricated in the university workshop. Selected specifications of the machine requiring power 240 V are given below. Force transducer type: strain gauge/piezoelectric, measurement of drop mass (maximum load = 80.5 kg): electrical with strain gauge load cell. Position transducer (max energy = 1603 J; min pressure = 0.414 MPa): optical encoder. Position accuracy: equal of less than ±0.2 mm or ±0.05% of displayed reading. Position repeatability: ±0.015 mm; speed accuracy: ±0.1% steady value. Velocity (max velocity = 20 m/s) detector display accuracy: ±0.25%; and velocity accuracy: ±2% of set value.

The laminates were tested mostly following the accepted American standard testing method for measuring damage resistance of a fibre-reinforced polymer matrix composite to a drop weight impact event (ASTM: D7136). The design of the testing was restricted to the analysis of low velocity below 5 m/s to avoid penetration. Prior to impacting, the laminate was tightly clamped around edges. As it is expected, these stable structures provided more logical experimental results. All tests were performed at room temperature. During each test, initial height was adjusted from the drop-weight height release levels to hit the laminate with a selected velocity at the centre of the laminate under the impactor head. To calibrate the brake system, the impactor was lowered to touch the surface of the laminate. Once the machine was set to its correct configuration and all data acquisition software running, the impactor was released to impact the laminate. Experiments start from minimal damage to the laminate under varied impact velocities ranging from approximately 1.6 to 4.3 m/s. Three different experiments were performed at the same impact velocity and the same conditions because there may be loose connection, defected samples or errors in sensors. Histories of impact loading were recorded using a PC-controlled high-speed A/D converter during every test.

5. Non-destructive damage inspection

Specimens were impacted at constant weight and different impact velocities to examine step by step damage. Results from relatively thin panel (8-Ply laminate) are well documented and are not being reported [1,8,10,15,18,26]. Similarly, Visual inspections and Eddy-current diagnosis methods provide quick and in-expensive general assessment but low velocity impact damage is internal and invisible. The C-scan maps of impacted laminates provide information on the damage mechanisms more particularly

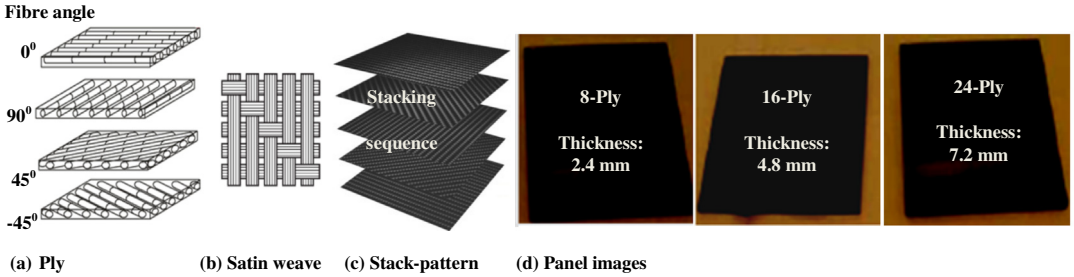

Fig. 1. Plies with fibre rotations, stain weave, stack, and laminated panels.

Table 1
Material properties.

Property	Units	Fibredux 914C-833-40
Tensile modulus (E_{11})	GPa	230
Tensile modulus ($E_{22} = E_{33}$)	GPa	21
Shear modulus (G_{12})	GPa	88
Out-of-plane shear modulus (G_{23})	GPa	11
Poisson's ratio (ν_{12})		0.33
Longitudinal tensile strength	MPa	1453
In-plane transverse strength	MPa	32
Longitudinal compressive strength	MPa	650
Out-of-plane transverse strength	MPa	15

to calculate the damage area which can be related to the load threshold and dissipation of energy during the impact. To correlate growth of impact induced damage in laminates up to the penetration, the impact induced damage areas need to be approximated. The amount of damage is quantified by the damage sustained area of the impacted laminate, approximated by counting the number of pixels occupied or meshing grids. A plane coordinate system is assumed to locate initial and final positions of the diameter of the damaged area. The damage length and width as shown in Fig. 4a radiating from the impact site at the centre is calculated by measuring distance with errors around 5% due to the ambiguous boundaries. The damaged area is assumed to map on ellipse/-circles by adding or subtracting rectangular mesh elements/cells (width: 8 and length: 6 are indicated by double arrows) as shown

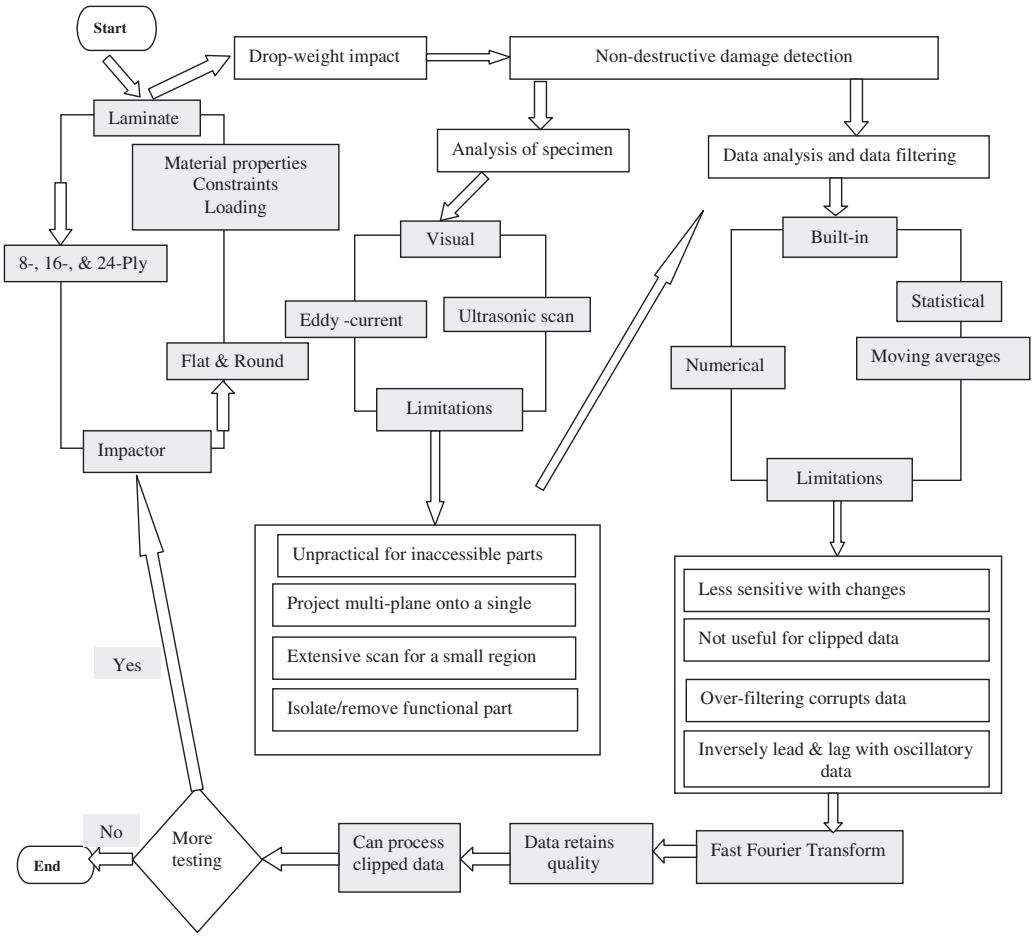

Fig. 2. Flowchart depicting stages of present work.

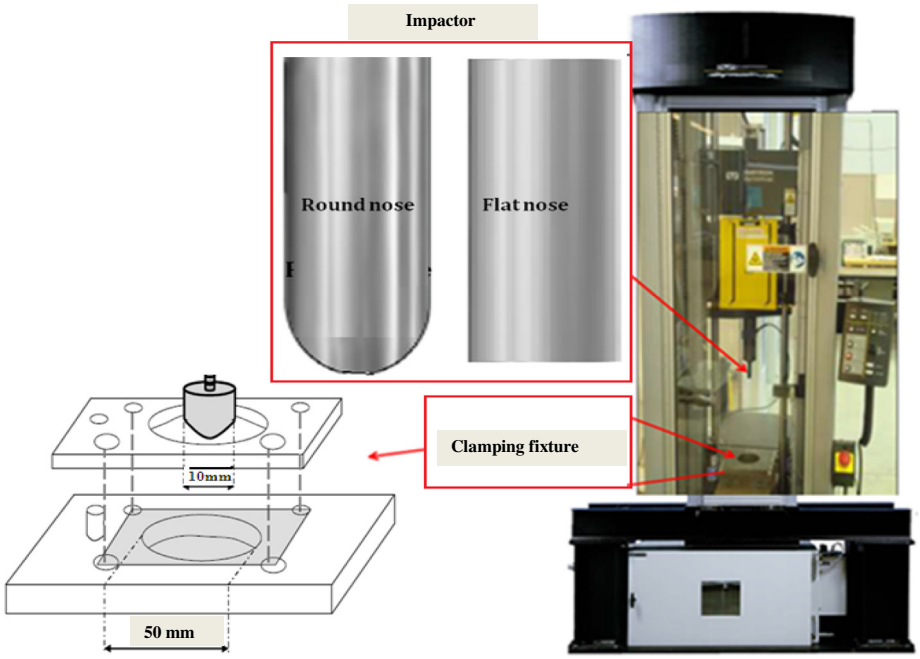

Fig. 3. INSTRON™ 9250 HV impact test machine.

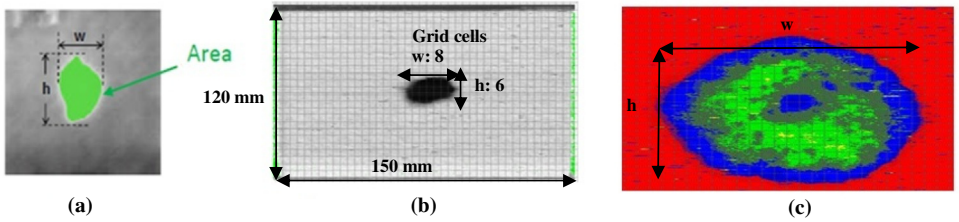

Fig. 4. Schematic of impact (a) damage area; (b and c) grid map of damage area.

in Fig. 4b. The damaged area is then divided by the laminate area to obtain an approximate damage percentage. Dimensions of the panels are defined in Fig. 1. Only visible damage can be approximated [26].

5.1. Comparison of results for 16-Ply laminates

Damaged areas detected by C-scan tests were approximated for 16-Ply panel of uniform scale as in Fig. 5a impacted at velocity: 1.7, 2, 2.2, 2.4, and 3.4 m/s by flat nose impactor. The figures show variations in damaged zones in the scanned images for five typical laminates subjected to increasing impact force levels. The approximated damaged area in each laminate corresponds to the impact loads that grew smoothly showing a relation between impact force and the damage size. In a relatively low loading case given in Fig. 5a and b, no obvious damage can be observed visually near contact zone at the laminate surface by naked-eyes though it existed inside the laminate as detected by scan. Furthermore, for impact with slightly higher impact load, increased damage can be observed in Fig. 5d and e. This indicates a direct proportion between the loading cases and the macroscopic damages.

5.2. Comparison of results for 24-Ply laminates

To further explore validation of the FFT filtered and extrapolated results, the 24-Ply laminates impacted at velocity range

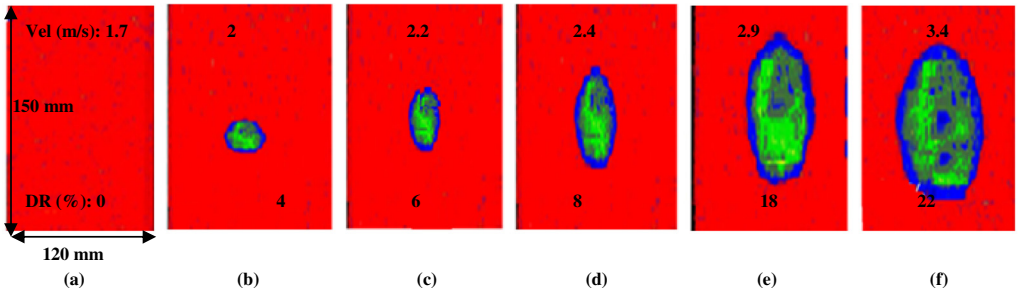

Fig. 5. C-scanned images of impact damaged are ratios (%).

3.1–4 m/s were selected for comparison. Similar discussion applies to the results. The comparison of C-scan detected approximate areas of 24-Ply laminate impacted by flat nose impactor are shown in Fig. 6a–f damage area ratios (21%) that corresponding plot is shown in Fig. 7 against load of 24 kN compares well to filtered results in depicted load 22 kN. In-plane scales of all the panels are the same as shown in Fig. 6a.

To visualise the relationship, the history of the load and damage quantities approximated by C-scan images were put together to observe the correlation in plot. Corresponding best-fit plot of load versus damage area ratios up to (23%) is shown in Fig. 7. The linear regression relation shows peak load value up to 25 kN to the (22–23%) damage area. The roughly linear relation between the damage area and load drop of the pulse correlates well for characterising the load threshold where damage initiates.

However, non-destructive inspections are limited as shown in Fig. 2.

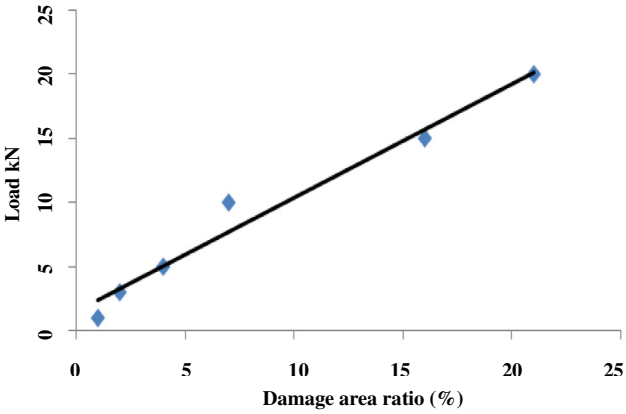

Fig. 7. Comparison of load versus C-scanned damaged area ratio (%).

6. Correlation of filtered data to load threshold

6.1. Load–deflection and load–time correlation to damage modes

During a weight-drop impact, the force–time curve includes significant oscillations with relatively close peak forces and intervals that complicate the characterisation of the delamination initiation and damage mechanisms. Thus, it is reasonable to consider the correlation between the damage size and the first impact force pulse (load threshold), such as its peak force, peak impact power, impulse, and transmitted impact energy. The maximum damage size of the laminate is expected to correlate mainly with the first impact force pulse such that the contribution of the subsequent pulses can be ignored. The load–deflection curves show the laminate's stiffness (slope of the curve), the maximum displacement and some information about absorbed energy (area under the curve). For the maximum impact energy, they globally divided the curve into four main parts [26]. The first part of the curve is linear and represents the stiffness of the non-damaged laminate. The second part of the load–deflection curve shows a load drop as a clear change in stiffness, indicating damage initiation. Third and fourth parts are concerned with through-thick and perforation. The proposed oscillations and changes in load–deflection curve due to fibre breakage, matrix cracks, de-lamination, and ply failure in plots of impact generated data were utilised to correlate and interpret threshold load of the impacted panels Fig. 8. Energy–time history traces can also be used to correlate and predict strain and elastic energy levels during impact event.

6.2. Data filtered with data acquisition system (built-in filters)

6.2.1. 8-Ply laminate versus impact velocities

Drop-weight impact tests were conducted out on 8-Ply laminate using flat nose impactors at velocity: 2.2, 2.41 and 3.12 m/s. Data recorded from two impact tests at velocity 2.2 m/s were filtered and plotted in Fig. 9a. Curves show consistent behaviour and a load drop at around 7 kN that indicates failure. Built-in filtered data recorded from impacts at velocity 2.41 and 3.12 m/s are plotted in Fig. 9b. Comparison of the plot shows different levels of curves for different impact velocities. Load drops around 5.5 kN indicate failure due to severe cracking Fig. 8. This indicates that the data acquisition system and built-in filter can gather and filter data for this range of impact velocities and laminates.

6.2.2. 8-Ply laminate versus impactor nose profiles

Drop-weight impact tests were conducted on 8-Ply laminate using flat and round nose impactors at velocity: 2.2 and 2.8 m/s. Data were recorded for two tests and filtered. Data from impact at velocity 2.2 m/s are plotted in Fig. 10a. The curve representing data plot from flat nose impactor shows a load drop around 7 kN while round nose curve shows a load drop around 3.5 kN [18]. Similarly, data from two tests were recorded and filtered from impact at velocity 2.8 m/s and plotted in Fig. 10b. The curve representing flat nose impactor shows a load drop at around 8 kN while round nose curve shows a load drop around 4 kN. The plot shows that flat nose impactor creates more damage than the round nose impactor when laminates are relatively thin. Consistent behaviour can be seen from the plots where load drops in all the cases indicate failure. This confirms that filtering the noisy data can be useful to interpret and analyse impact behaviour of laminated composites for this range.

6.2.3. Comparison of velocity, load, and deflection history

Graphical comparisons of the test generated and filtered data were correlated to the irregularities in applied load to interpret useful information about how the material behaves during the

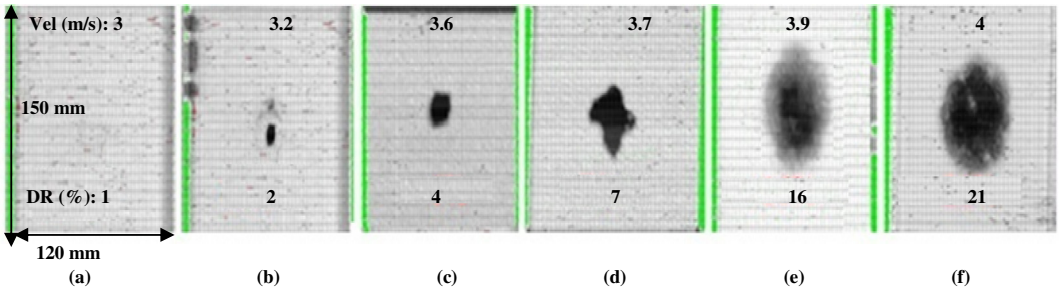

Fig. 6. C-scanned images of 24-Ply panels: velocity versus damage area ratio (DR: %).

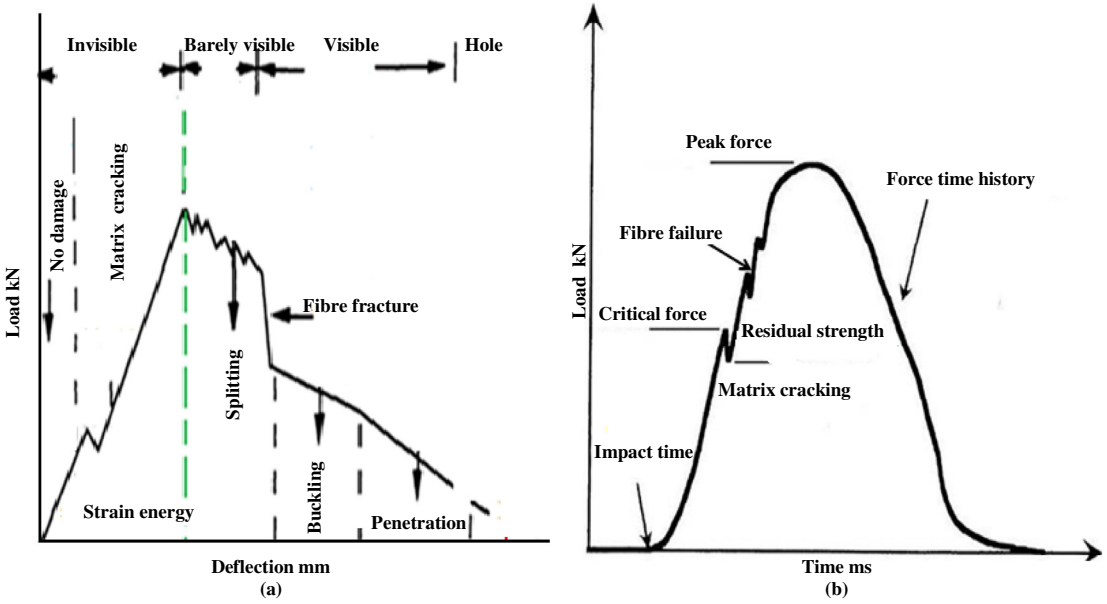

Fig. 8. Schematic of possible damage modes.

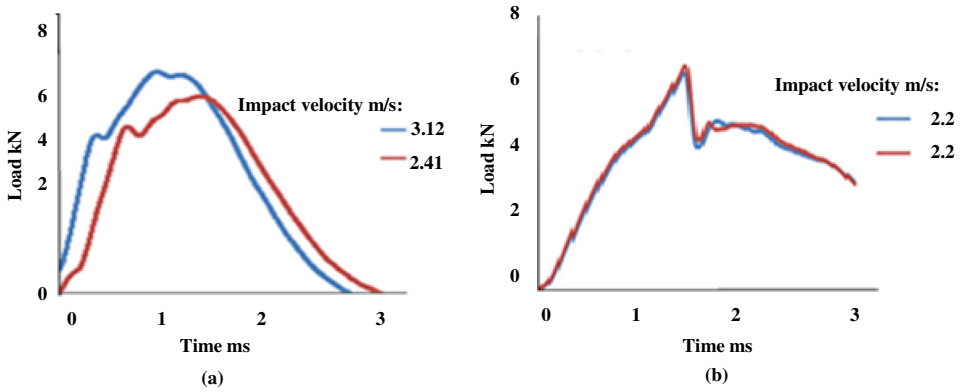

Fig. 9. Load–time history of 8-Ply laminate: (a) same, (b) different velocities.

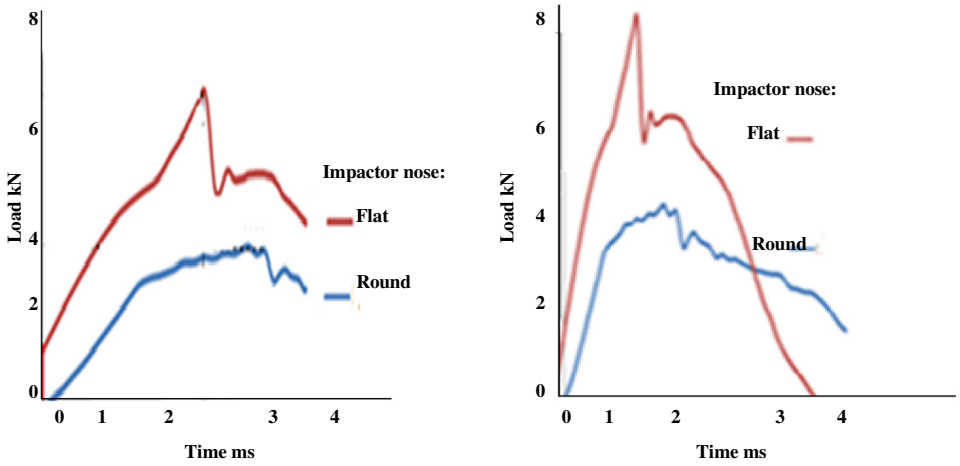

Fig. 10. Load–time response of 8-Ply panels under different impactor nose profiles.

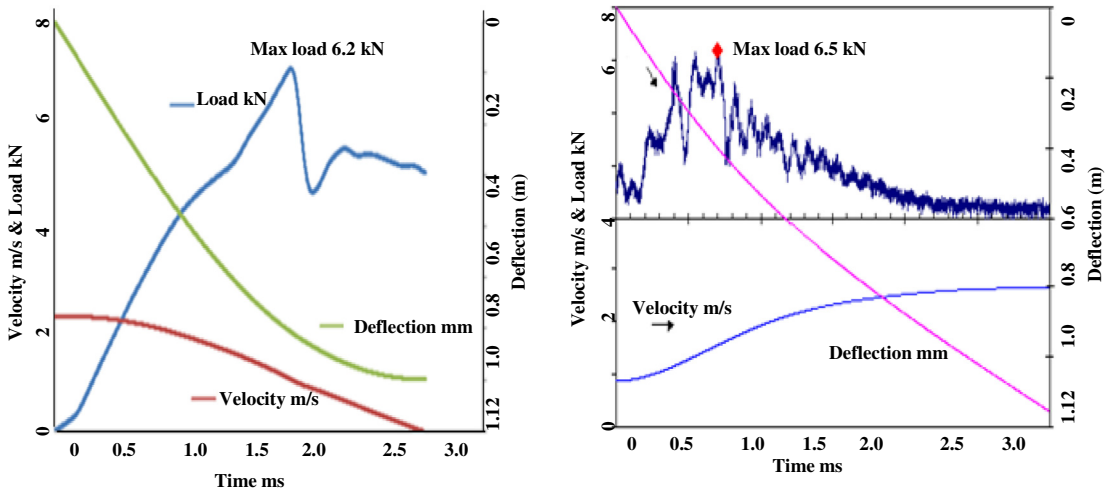

Fig. 11. Velocity–, load– and deflection–time history compared to data in [1].

impact process. Selected plot of deflection curves under flat nose impact of 8-Ply laminate at velocity 2.2 m/s trace in Fig. 11a were compared to curves in Fig. 11b [1]. Both the results show a severe load drop at around 7 kN that indicates ply level failure. This confirms that prediction of threshold load from interpretation of recorded and filtered data of the impact events are reliable and realistic.

Drop-weight impact tests were performed to investigate influence from the flat and round nose impacts of 8-Ply laminates of at velocity 1.6 m/s. The test generated data were recorded during the impact process and column-chart was plotted. No sudden/abrupt fluctuation of load drop can be seen from column-chart for both the impactor shapes. The comparison of load–deflection quantities created from the flat and round nose impactors is shown in Fig. 12. This confirms that impact-induced damage from round and flat nose impactors do not show much difference for the impact velocity range up to 1.6 m/s using built-in filters.

Based on the comparisons, supported by the non-destructive methods [26], the limitations could be attributed to: low velocity range, thin laminate, impacting machine, and data logging systems. Since data gathered and filtered by built-in system with the velocity range below 1.7 m/s of 16-Ply and 24-Ply laminates have also shown similar limitations hence results for these panels are not reported.

6.3. Data filtering with statistical methods

Moving average method is the widely used statistical method for data filtering and data extrapolation in science and engineering applications. Common moving average (smoothing) methods are: moving averages, weighted moving averages, and centred moving average. Higher order methods can be used to smooth large amounts of oscillatory and for missing data. The moving averages method consists of computing an average of the most recent data values for the series and using this average to predict the value of the time series for the next period. Cases in which time series is fairly stable one can use such smoothing methods to average out the irregular component of the time series. Moving averages are useful if it is assumed that the item to be predicted stays fairly steady over time designed. To predict the missing value a three-point moving average method was utilised [26].

6.3.1. 16-Ply laminate impacted versus impactor nose profiles

Drop-weight impact tests were conducted on 16-Ply laminate using flat and round nose impactors at velocity: 3.12 m/s.

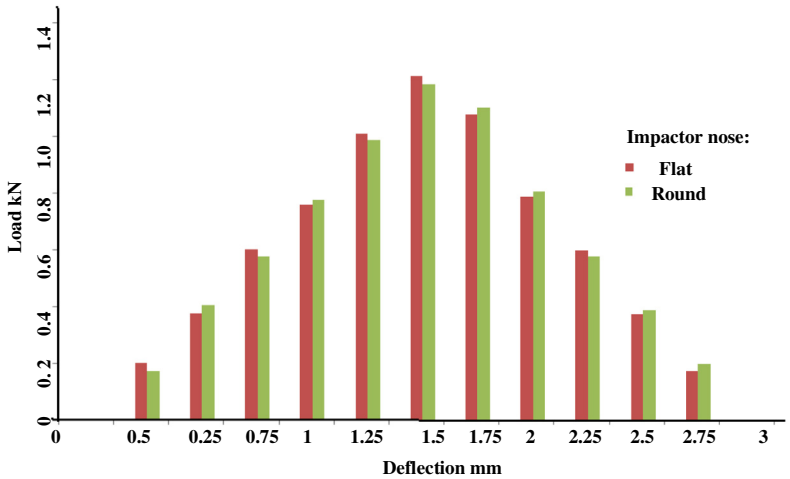

Fig. 12. Load–deflection response of 8-Ply impacted at velocity 1.6 m/s.

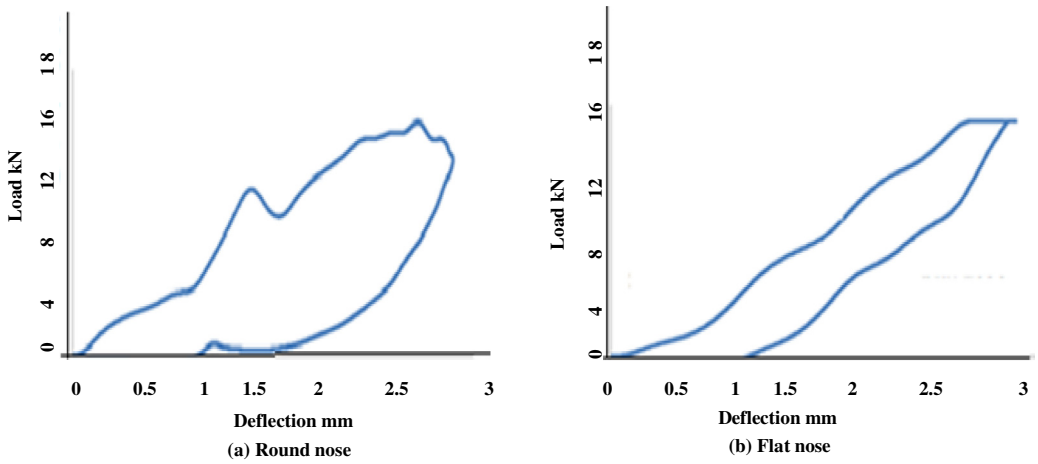

Fig. 13. Load–deflection response of 16-Ply panel with round and flat nose impacts.

Recorded data were filtered and are plotted in Fig. 13a and b that depicts closed loops. The elastic impact and rebound curve for round nose shows consistent behaviour to some extent, the load drops around 11 kN that indicates failure. However, filtered data gathered from flat nose impact show slightly inconsistent behaviour. Instead of load drop it shows negligible constant loading line like plastic behaviour after load range 14 kN.

6.3.2. 24-Ply laminates impacted versus impactor nose profiles

Drop-weight tests were performed on 24-Ply laminates impacted by flat and round nose impactors at impact velocity 3.74 m/s. Data filtered and recorded by built-in data acquisition system were plotted. Fig. 14 shows load drop after 13 kN in curve representing round nose impact while inconsistent tendencies after 17 kN can be seen in curve that represents flat nose impact. A straight horizontal line is recorded after peak the load when a load drop was expected indicates a constant resistance of the laminate to the applied load. This could be due to the laminates' larger thickness and flat nose of the impactor. Generally, thickness factor increases proportional to the flexural rigidity that causes a dissipation of impactor energy into absorbed energy and frictional noise between laminate and impactor.

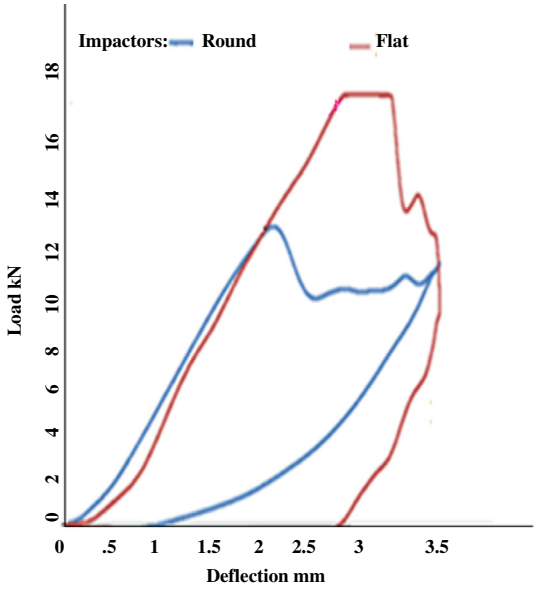

Fig. 14. Load–deflection of 24-Ply laminate impacted versus impactor nose profiles.

6.3.3. Comparison of velocity, load, and deflection history

Comparisons of the test generated data for 24-Ply laminate impacted by flat and round nose impactors at velocity 3.74 m/s are plotted in Fig. 15a and b. Curves relating to flat nose impact for velocity and deflection parameter also show consistent behaviour. However, load history shows an inconsistent behaviour and no load drop. The comparison of round nose data plot also shows similar patterns and trends. Based on the results of comparison it can be argued that data generated from such impact events cannot be readily filtered using conventional data filtering techniques.

The moving average process lags behind increasing data and leads the decreasing data values. The methods require sufficient historical data values. Some of the other limitations of the statistical methods are shown in Fig. 2.

6.4. Data filtering using numerical techniques

More reliable and robust methods are based on numerical analysis techniques. Extrapolation of numerical values consists of using the curve fitting techniques to estimate data quantities and then extend predictions based upon the estimated data [26]. The widely used algorithms are numerical integrations that could more reliably lead to a band of future quantities. One such method is the modified Simpson's rule regarded as inherent filter. Simpson's rule is a method of finding areas under a curve using an approximate integration method. The next part of Simpson's rule is regression. This results in an equation for velocity that can be used to calculate other values such as displacements by similar integration. The other value that can be obtained from this is the force if mass of free falling weight and the acceleration are known. The modified Simpson's rule was selected for data filtering herein. As interval $[a, b]$ is split up in n sub-intervals, with n an even number where equidistant x values are $x_0, x_1, \ldots, x_n$ the step width being $h = \frac{(b-a)}{n}$. The composite Simpson's rule given by the 2nd order polynomials (parabolas) for approximating the curve to be integrated can be written as:

$$\int_a^b [f(x)]dt \approx \frac{h}{3}\left[(f(a)+f(b)) + 2\sum_{k=1}^{n/2^{-1}} f(x_{2k}) + 4\sum_{k=1}^{n/2} f(x_{2k-1})\right] \quad (1)$$

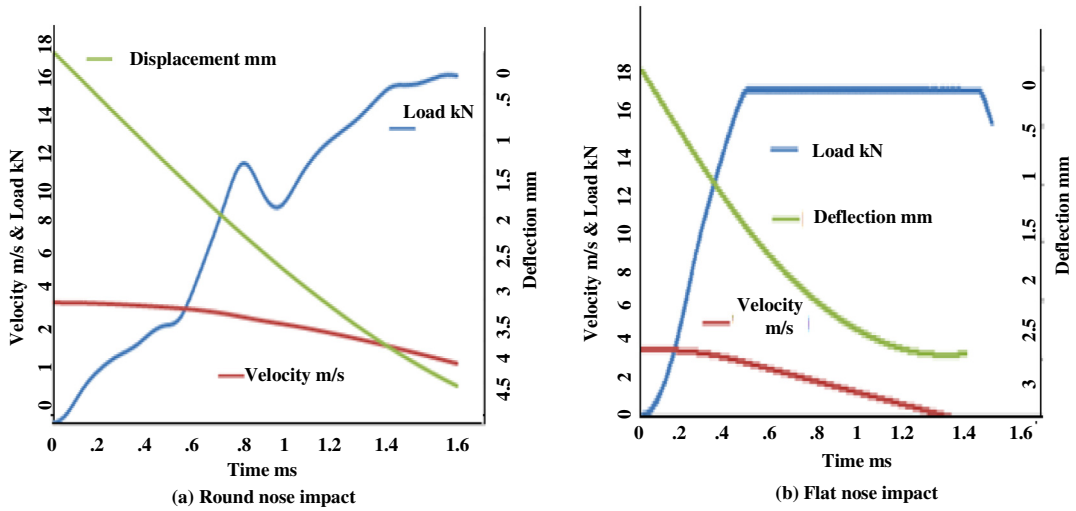

Fig. 15. Velocity–, load–, and deflection– time history of 24-Ply laminate.

The area needs to be divided into equally spaced intervals of uniform width. The algorithm uses Eq. (1) to compute area:

$$\text{Area} = \frac{h}{3}(A + 2B + 4C) \tag{2}$$

where a, b are first and last values of the given sequence and k varies from 1 to the total number of points N in the sequence. A is sum of first and last ordinates; B is the sum of remaining ordinates, and C is the sum of even ordinates and h is width of a strip. Application of the algorithm is illustrated for the flat nose impact of 24-Ply panels impacted at velocity 3.74 m/s in plots of Fig. 16 below.

6.4.1. Energy–time history of 24-ply laminate impacted with 3.74 m/s

The energy–time history traces show influence of impactor nose profiles in respect of impact-induced damage. It can be seen that despite the same velocity both the impactors attain slightly different impact energy levels Fig. 16. Looking at the curves the increased impact energy, absorbed (two phases), elastic energy zones depict the difference. The energy absorbed by the panel during impact can be quantified by evaluating the area under the curve. The impact energy converted to elastic vibrations has also been reversed for different nose profiles. This can be attributed to the thickness of the laminates. Impact energy history curve representing round nose impact shows exceeded elastic/vibration energy phase. The laminate in such case (impacted by round nose) absorbs more energy through converting the impact energy into elastic vibrations. Thus, the laminate impacted by round nose generates high elastic energy that results in more failure modes and mechanisms. Moreover, a small change (kink) in the curves rate can also be seen in the curve representing impact from the flat nose at around 14 J. This negligibly small change can be attributed to the flexure deformation of the laminate. Impact, elastic, and absorbed energy levels depicted in the plot with using numerical filters indicate recorded data were genuine and could be used to interpret the impact response.

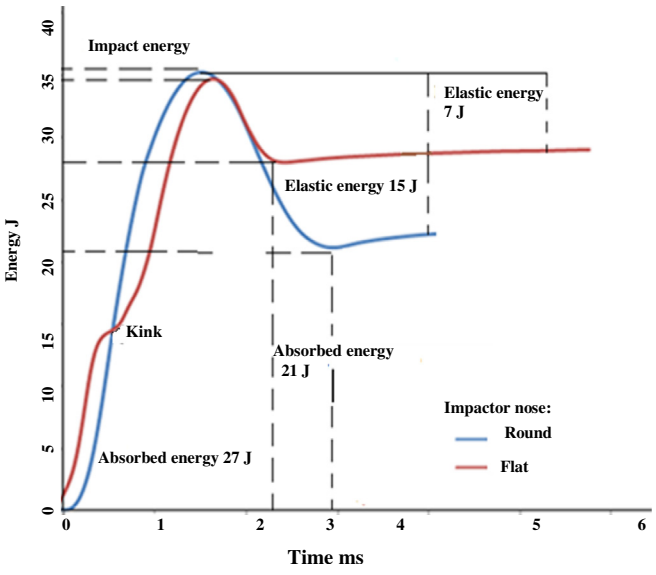

Fig. 16. Energy history of 24-Ply laminate impacted at velocity 3.74 m/s.

6.4.2. Load–time history of 16-, 24-ply laminate impacted with 3.74 m/s

To further confirm the inconsistent behaviour, data from round and flat nose impact tests of 16- and 24-Ply laminates were recorded, filtered, and plotted in Fig. 17a and b. Consistent and expected behaviour was observed in velocity, deflection, and energy history time plots. Load–time histories were found to be as expected. However, the elastic impact curves for flat nose impactor of 24-Ply laminates show inconsistent behaviour to some extent and load curves show plastic type behaviour near 17 kN. The inconsistent behaviour in load–time plot before reaching 80 kN of machine's specification cut-off of frequency indicates limitations of data logging and impact system. This could be attributed to the flat nose type of impactor and relatively thick laminates consisting of 24-Ply. The data of Fig. 17b were filtered utilising numerical algorithms but not much improvement was achieved.

The numerical filtering process is complicated and involves a combination of numerical methods to reach a reliable future value. Parts of data consisting of little interference or noise and parts of significant peaks could be lost due to heavy filtering. Removal of force and energy from critical regions will give rise to incorrect quantitative data during further analysis. Numerical integration requires reliable initial value to predict next estimates. Moreover, numerical method based filters cannot readily improve data-bands consisting of straight lines (slope is zero). Useful information cannot be extracted from data plots due to narrow band of data points for slope of clipped-data.

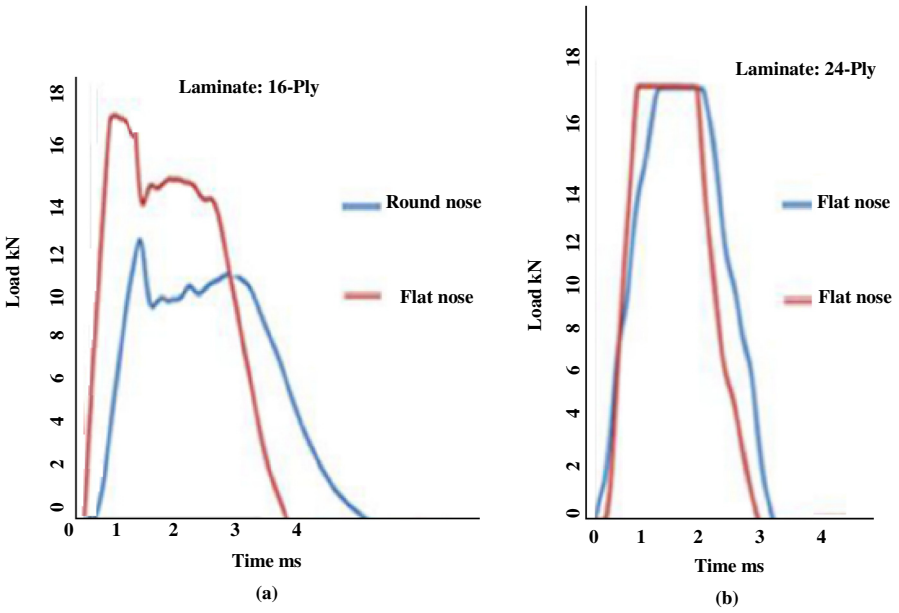

Fig. 17. Load–time traces of 16-, 24-Ply laminates versus impactor nose profiles.

7. Advanced data filtering methods

7.1. Fast Fourier algorithms

The fast Fourier algorithm is widely used in solving many engineering challenges, designing filters, performing spectral analysis, estimation, noise cancellation and benchmark testing devices and systems. The algorithm considerably reduces time taken to evaluate a discrete Fourier transform (DFT) on a digital computer and depends on the number of multiplications involved in the slowest operations, particularly when high number of sample is involved. The standard DFT involves a lot of redundant calculations and forces one further assumption that number of data points (N) is an integer multiple of 2. This allows certain symmetries to occur reducing the number of calculations. e^{jw_0t}: time-varying term has unit magnitude and rotates counter-clockwise in the complex plane at a rate of w_0 rad/s ($f_0$rotations/s). Maximum frequency ($f_{\max}$) depends on the sampling interval and the frequency resolution determined by the signal record length. The N samples of a time signal recorded during a finite duration of T with a sampling period of Δt ($N = T/n\Delta t$) can be transformed into samples in the frequency domain between $-f_{\max}$ and $+f_{\max}$ according to:

$$f_{\max} = \frac{1}{2\Delta t}, \quad \Delta f = \frac{1}{T} \tag{3}$$

Roots of unity (w) and periodic symmetry facilitate to compute the root once and split it into odd and even using basic relations $e^{n\pi i} = \cos n\pi + i \sin n\pi = (-1)^n$ shown in Fig. 18.

Given N, the N-point DFT of $x[n]$ is defined as a vector, where it could also be readily useable for computing the inverse transforms as:

$$X[k] = \sum_{n=0}^{N-1} x[n] e^{-j\frac{2\pi}{N}nk} \quad \text{for } k = 0, 1, 2, \ldots, N-1 \tag{4}$$

To compute the DFT, we use only the values: $x[0],\ x[1],\ \ldots,\ x[N-1]$. Hence if the signal is non-zero outside this range of n, the DFT loses some information. However, if the non-zero only for $n = 0,\ 1,\ \ldots,\ N-1$ we recover it from $\{X[k]\}$ via the formula:

$$x[n] = \frac{1}{N} \sum_{n=0}^{N-1} X[k] e^{j2\pi nk/N}, \quad k = 0,\ 1,\ \ldots,\ N-1 \tag{5}$$

The algorithm rearranges the DFT series into two parts: a sum over the even numbered discrete-time indices $n = [0,\ 2,\ 4,\ \ldots,\ N-2]$ and a sum over the odd numbered indices $n = [1,\ 3,\ 5,\ \ldots,\ N-1]$. This is called decimation in time because the time samples are rearranged in alternating groups, each with length $N/2$, by grouping even and odd-indexed samples proceed as:

$$X[k] = \sum_{n=0}^{N-1} x[n] W_N^{nk} = \sum_{n=\text{odd}} x[n] W_N^{nk} + \sum_{n=\text{even}} x[n] W_N^{nk} \tag{6}$$

Let $n = 2r$ in the first and $n = 2r + 1$ in the second sum:

$$X(k) = \sum_{r=0}^{N/2-1} x[2r] W_N^{2kr} + \sum_{r=0}^{N/2-1} x[2r+1] W_N^{(2r+1)k} \quad \text{with } g[r] = x[2r]h[r] = x[2r+1] \tag{7}$$

The $N/2$-point terms uses symmetry and the identities:

$$W_{N/2} = e^{-j\frac{2\pi}{N/2}} = e^{-j\frac{2\pi^2}{N}} = \left(e^{-j\frac{2\pi}{N}}\right)^2 = W_N^2. \tag{8}$$

The W_N (nth root of unity) values are the coefficients of the FFT and are often referred to as twiddle factors (complex exponential values). Because of its shape the basic computational unit of the FFT is called a butterfly (because of its crisscross appearance), simplified by factoring out a term W_N^{nk} from the lower branch as illustrated in Fig. 19. The factor that remains is $W_N^{N/2} = -1$. Each of the building blocks has the following structure:

The FFT algorithm provides spectral components of signals between 0 and 0.5 sampling frequencies that require less computational time and effort than DFTs. It passes the spectral contents of an input data/signal in a certain band of frequencies filtering transfer functions in the frequency domain window as filters which include low pass, high pass, band pass, and band stop to selectively change the wave shape, amplitude and frequency characteristics of a signal in a desired manner. Use of transfer function allows ratios of output and input noise to be separated and removed from the original data so as to build a clear image of true

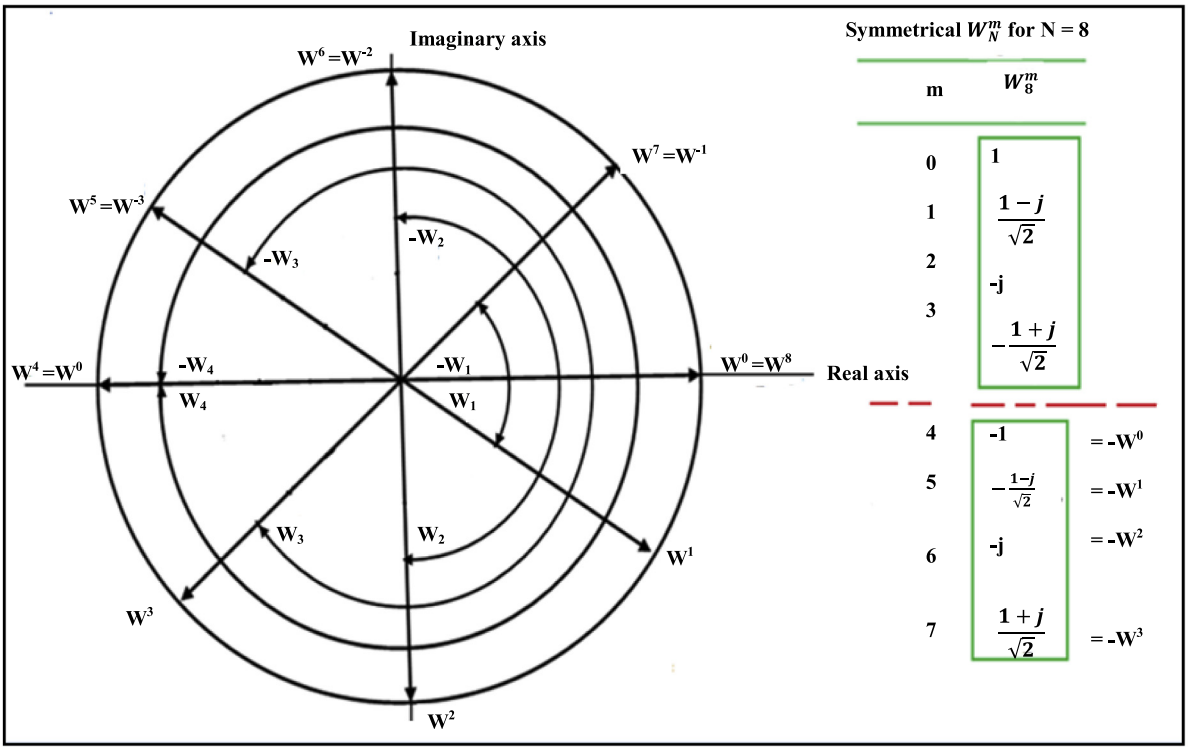

Fig. 18. Computational symmetry & data split in even and odd sub-sequences.

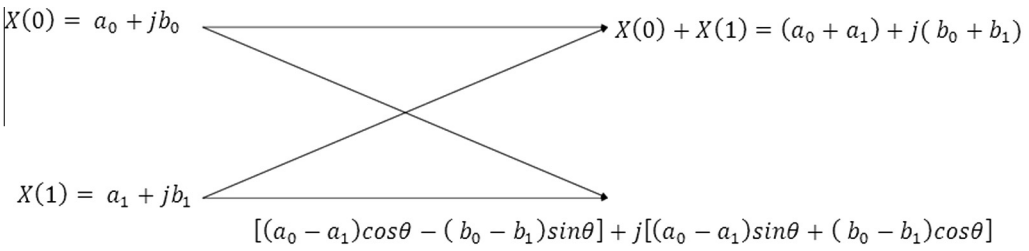

Fig. 19. Schematic of possible values at first and second stages.

data. Proceeding with the transformation to obtain transfer function the algorithm can be re-written in gain form by suppressing low and upper limits:

$$G[iw] = \int g(t)e^{-iwnt} \tag{9}$$

and integrating by parts produces:

$$G[iw] = e^{-iwnt}\left(\left(\frac{g(t)^2}{2}\right) + \frac{1}{-iwn}\right) + c \tag{10}$$

Assuming $c = -1$ and $e^{-iwnt} \approx 1$ gives by multiplying the top and bottom by $2 - iwn$ and re-factoring:

$$G[iw] = \frac{g(t)^2}{2 - wn} \tag{11}$$

This is the transfer function from the time domain to the frequency domain. To convert back to the time domain the function uses:

$$g(t) = \frac{1}{2\pi}\int G[iw]e^{-iwnt} \tag{12}$$

where $G[iw]$ is called phase of the system; jw is the phasor notation of s; and $g(t)$ is the input signal/information. Hence a given system defined by its impulse response $h(t)$, the output, $y(t)$ can be found by convolving the input $x(t)$ with the Laplace transform (low case change to upper case and t changes to s) as:

$$Y(s) = H(s)X(s). \tag{13}$$

It shows convolution in the time domain is equivalent to multiplication in the Laplace domain. Replacing s by Ω, the equation can be obtained as:

$$Y(\Omega) = H(\Omega)X(\Omega) \tag{14}$$

which describes the frequency response of the system where $Y(\Omega)$ indicates output, $X(\Omega)$ the input and $H(\Omega)$ as the filter. For a signal $x[n]$, the DFT $X(\Omega)$ it is a 2π – periodic function of continuous variable, the frequency Ω. The sampling frequency $f_s = \frac{1}{T_s}$ (in Hz) or $\Omega_s = \frac{2\pi}{T}$ (in rad/s). Magnitude of the transfer function, $|H(\Omega)|$, is considered when the characteristics of various filters are studied that maps time domain and frequency domains through Fourier Transform. Once the input and output signal have been converted from time domain to the frequency domain further manipulation is required to put the data into a suitable format so that filtering can take place. The convolution integral can be difficult to deal with because of the time shift. But, the Laplace transform for the convolution integral turns it into a simple multiplication.

7.2. Circular convolution of Fourier algorithms to filter data

The Fourier methods transform data into circular domain and transform non-periodic data into periodic forms. Hence, periodic convolution of Fourier filter alters the frequency response (both magnitude and phase) of a signal. The sample sequence of complex values: $\{x[nT]\} = x[0], x[T], \ldots, x[(N-1)T]$ where n is the sample number from $n = 0$ to $N-1$ can be periodically sampled at regular time intervals T to form a circle (waveform). The process of filtering the circular sequence in time domain is called convolution. The Fourier transform can be considered to be a bank of band-pass filters that takes in a signal and the magnitude of the output. Each of the filters convolves input with a set of filter coefficients (sinusoidal in nature) with the frequency of oscillation equal to the centre frequency of the filter. The relationship between the input $x(t)$ and output $y(t)$ signals of invariant systems is described in terms of the impulse response $h(t)$ of the system. The time invariant system can be completely characterised by its impulse response applied (at time $t = 0$ or $n = 0$). This is easily achieved in the discrete time convolution where the input is set equal to an impulse $\delta(n)$ where an arbitrary input signal can be expressed as the weighted superposition of time shifted impulses $x(t) = x(\tau)\,\delta(t-\tau)$ where τ varies and responses as:

$$y(t) = \int_{\tau=-\infty}^{t} h(t-\tau) \times (\tau)d\tau = \int_{0}^{\infty} h(\tau) \times (t-\tau)d\tau \tag{15}$$

Digital systems require that the convolution sum replaces the convolution integral and is defined by:

$$y(n) = \sum_{k=-\infty}^{\infty} x(k)h(n-k) \tag{16}$$

Moreover, to be tractable $x(n)$ and $h(n)$ are nonzero only over a finite interval and the variable τ known as singularity shifts the function if it is nonzero.

$$Y(k) = X(k)H(k) \tag{17}$$

$$\begin{aligned} y[n] = \mathrm{IDFT}\{Y\{k\}\} &= \frac{1}{N}\sum_{k=0}^{N-1} Y(k)e^{j\frac{2\pi}{N}nk} = \frac{1}{N}\sum_{k=0}^{N-1} X(k)H(k)e^{j\frac{2\pi}{N}nk} \\ &= \frac{1}{N}\sum_{k=0}^{N-1}\left\{\frac{1}{N}\sum_{k=0}^{N-1} h(m)e^{-j\frac{2\pi}{N}mk}X(k)e^{j\frac{2\pi}{N}nk}\right\} \\ &= \sum_{m=0}^{N-1} h[m] \times [n-m] \text{ Discrete Fourier in two sequences.} \end{aligned} \tag{18}$$

The sequence values need not be sampled at a rate which is at least double the highest significant frequency component of the signal (known as the Nyquist rate). If the signal is not sampled at least twice the frequency of the highest frequency component, the high frequency signals are aliased down to a lower frequency. In most applications, an anti-aliasing (low-pass) filter is used to attenuate unwanted data prior to sampling. In the time domain the process of filtering is a convolution:

$$y(t) = x(t) \otimes h(t) \tag{19}$$

where $y(t)$ denotes the output signal; $x(t)$ the input signal; $h(t)$: the impulse response of the filter and $\otimes$ denotes convolution. Input of a perfect impulse (i.e., a delta function) is,

$$h(t) = \delta(t) \otimes h(t) \tag{20}$$

Eqs. (16) and (17) are related by the Fourier Transform (F) as:

$$\begin{aligned} Y(\Omega) &= F[y(t)] \\ X(\Omega) &= F[x(t)] \\ H(\Omega) &= F[h(t)] \end{aligned} \tag{21}$$

In the frequency domain the filtering process is a simple case of multiplication Eq. (14). The inverse Fourier Transform (F^{-1}) gets us from the frequency to the time domain:

$$\begin{aligned} y(t) &= F^{-1}[Y(\Omega)] \\ x(t) &= F^{-1}[X(\Omega)] \\ h(t) &= F^{-1}[H(\Omega)] \end{aligned} \tag{22}$$

Eq. (15) above is for continuous (analogue) signals and filters. The equivalent for discrete (digital) systems is:

$$y_n = \sum_{k=0}^{2m-1} x_k \otimes h_k. \tag{23}$$

The algorithms recursively partitions a sequence into two half-length sequences of even and odd-indexed time samples. The outputs of these shorter sequences are reused to compute many outputs, thus greatly reducing the total computational cost.

7.3. Implementation of the data filtering algorithms

The decimation-in-time FFT algorithm, the butterfly computation requires only $N/2$ twiddle-factor multiplies per stage. The same radix-2 decimation-in-time can be applied recursively to the two $(N \times N)$ length N^2 DFTs to save computation. Shuffling of the input sequence takes place due to the successive decimations of $x[n]$. Instead of directly evaluating coefficients $a_k and b_k$ the coefficients:

$$c_k = \frac{1}{m}\sum_{k=0}^{2m-1} c_k e^{ikx} \quad \text{where } c_k = \sum_{j=0}^{2m-1} y_j e^{\pi i j\frac{k}{m}},\ k = 0, 1, \ldots, 2m-1 \tag{24}$$

are computed first.

Once the constants c_k were determined, a_k and b_k could be recovered. The integer nk repeats for different combinations of k and n; secondly W_N^{nk} is a periodic function with only N distinct values. Considering $N = 8$ the FFT, it can be seen that: $W_8^4 = -W_8^0$, $W_8^5 = -W_8^1$, $W_8^6 = -W_8^2$, $W_8^7 = -W_8^3$. Also, if nk falls outside the range 0–7, it still gets one of the above values. The N-point DFT can be obtained from two $N/2$-point transforms, one on even input data $G(k)$ and one on odd input data $H(k)$.

$$X(k) = G(k) + W_N^k H(k) \tag{25}$$

Although the frequency index k ranges over N values, only $N/2$ values of $G(k)$ and $H(k)$ need to be computed since they are periodic in k with period $N/2$. Where n is the sample number from $n = 0$ to $N-1$ and index k ranges over N values. There were 16,000 data points for each drop-weight tests. The original twiddle matrix is of 16,000 by 16,000 in MATLAB™ code corresponding to test generated data points. Selecting 8 points from the start of the clipped data for $N = 8$ the algorithm proceeds splitting the input data points in even $f[0]\ f[2]\ f[4]\ f[6]$ and odd sequences $f[1]\ f[3]\ f[5]\ f[7]$ using Eq. (25):

$$\begin{aligned} X[0] &= G[0] + W_8^0 H[0] \\ X[1] &= G[1] + W_8^1 H[1] \\ X[2] &= G[2] + W_8^2 H[2] \\ X[3] &= G[3] + W_8^3 H[3] \\ X[4] &= G[4] + W_8^4 H[4] = G[0] - W_8^0 H[0] \\ X[5] &= G[5] + W_8^5 H[5] = G[1] - W_8^1 H[1] \\ X[6] &= G[6] + W_8^6 H[6] = G[2] - W_8^2 H[2] \\ X[7] &= G[7] + W_8^7 H[7] = G[3] - W_8^3 H[3] \end{aligned}$$

Hence, a typical computation procedure applied to $8 = 2^3$ data points is described for direct calculations of the complex constants in the 4 steps. The algorithm computes complex constants c_k for a 8-data points $\{(\mathbf{x_j y_j})\}_0^7$ as follows:

Step 1:

$$c_k = \sum_{j=0}^{2m-1} y_j e^{\pi i j \frac{k}{m}}, \quad k = 0,\ 1,\ \ldots,\ 2m-1.$$

$$c_0 = y_0 + y_1 + y_2 + y_3 + y_4 + y_5 + y_6 + y_7$$

$$c_1 = y_0 + \left(\tfrac{(i+1)}{\sqrt{2}}\right)y_1 + iy_2 + \left(\tfrac{(i-1)}{\sqrt{2}}\right)y_3 - y_4 - \left(\tfrac{(i+1)}{\sqrt{2}}\right)y_5 - iy_6 - \left(\tfrac{(i-1)}{\sqrt{2}}\right)y_7$$

$$c_2 = y_0 + iy_1 - y_2 - iy_3 + y_4 + iy_5 - y_6 - iy_7$$

$$c_3 = y_0 + \left(\tfrac{(i-1)}{\sqrt{2}}\right)y_1 - iy_2 + \left(\tfrac{(i+1)}{\sqrt{2}}\right)y_3 - y_4 - \left(\tfrac{(i-1)}{\sqrt{2}}\right)y_5 + iy_6 - \left(\tfrac{(i+1)}{\sqrt{2}}\right)y_7$$

$$c_4 = y_0 - y_1 + y_2 - iy_3 + y_4 - y_5 + y_6 - y_7$$

$$c_5 = y_0 - \left(\tfrac{(i+1)}{\sqrt{2}}\right)y_1 + iy_2 - \left(\tfrac{(i-1)}{\sqrt{2}}\right)y_3 - y_4 + \left(\tfrac{(i+1)}{\sqrt{2}}\right)y_5 - iy_6 + \left(\tfrac{(i-1)}{\sqrt{2}}\right)y_7$$

$$c_6 = y_0 - iy_1 - y_2 + iy_3 + y_4 - iy_5 - y_6 + iy_7$$

$$c_7 = y_0 - \left(\tfrac{(i-1)}{\sqrt{2}}\right)y_1 - iy_2 - \left(\tfrac{(i+1)}{\sqrt{2}}\right)y_3 - y_4 + \left(\tfrac{(i-1)}{\sqrt{2}}\right)y_5 + iy_6 + \left(\tfrac{(i+1)}{\sqrt{2}}\right)y_7$$

Step 2:

$$d_0 = \tfrac{1}{2}(c_0 + c_4);\ d_1 = \tfrac{1}{2}(c_0 - c_4);\ d_2 = \tfrac{1}{2}(c_1 + c_5);\ d_3 = \tfrac{1}{2}(c_1 - c_5);$$
$$d_4 = \tfrac{1}{2}(c_2 + c_6);\ d_5 = \tfrac{1}{2}(c_2 - c_6);\ d_6 = \tfrac{1}{2}(c_3 + c_7);\ d_7 = \tfrac{1}{2}(c_3 - c_7)$$

Step 3:

$$e_0 = \tfrac{1}{2}(d_0 + d_4);\ e_1 = \tfrac{1}{2}(d_0 - d_4);\ e_2 = \tfrac{1}{2}(id_1 + d_5);$$
$$e_3 = \tfrac{1}{2}(id_i - d_5);\ e_4 = \tfrac{1}{2}(d_2 + d_6);$$
$$e_5 = \tfrac{1}{2}(d_2 - d_6);\ e_6 = \tfrac{1}{2}(id_3 + d_7);\ e_7 = \tfrac{1}{2}(id_3 - d_7)$$

Step 4:

$$f_0 = \tfrac{1}{2}(e_0 + e_4);\ f_1 = \tfrac{1}{2}(e_0 - e_4);\ f_2 = \tfrac{1}{2}(ie_1 + e_5);\ f_3 = \tfrac{1}{2}(ie_1 - e_5);$$
$$f_4 = \tfrac{1}{2}\left(\left(\tfrac{(i+1)}{\sqrt{2}}\right)e_2 + e_6\right);\ f_5 = \tfrac{1}{2}\left(\left(\tfrac{(i+1)}{\sqrt{2}}\right)e_2 - e_6\right);$$
$$f_6 = \tfrac{1}{2}\left(\left(\tfrac{(i-1)}{\sqrt{2}}\right)e_3 + e_7\right);\ f_7 = \tfrac{1}{2}\left(\left(\tfrac{(i-1)}{\sqrt{2}}\right)e_3 - e_7\right)$$

Defining:

$$F(x) = \frac{1}{4}\sum_{k=0}^{3} c_k e^{ikx} \text{ where } c_k = \sum_{k=0}^{3} y_j e^{ijx} \tag{26}$$

So $\frac{1}{8}c_k e^{-ikx} = a_k + ib_k$ for k = 0, 1, 2, …, $2m-1$ and 2 m = 8.

Using divide and conquer algorithm:

$$c_k + c_{k+m} = \sum_{j=0}^{2m-1} y_j e^{ij\left(\pi\frac{k}{m}\right)} + \sum_{j=0}^{2m-1} y_j e^{ij\pi\left(\frac{m+k}{m}\right)}$$
$$= \sum_{j=0}^{2m-1} y_j e^{ij\pi\left(\frac{k}{m}\right)}(1 + e^{ij\pi}) \text{ for } k = 0,\ 1,\ 2,\ \ldots,\ m-1 \tag{27}$$

where:

$$1 + e^{ij\pi} = \begin{cases} 2 \text{ if } j \text{ is seven} \\ 0 \text{ if } j \text{ is odd.} \end{cases} \tag{28}$$

As N is a power of 2, the above process on the two $N/2$-point transform were repeated, breaking them down to $N/4$-point transforms, etc until we came down to 2-point transforms. For $N = 8$, only one further stage was needed. Once operation performed on a pair of complex numbers, there was no need to save the input pair. Therefore, the output pair was stored in the same registers as the input. Thus, only one array of size N was required. The computations were performed in-place, the input sequence that $x[n]$ stored in non-dimensional order. For 1024 samples data sequence, the DFT requires N^2 complex multiplications for a matrix of $1024 \times 1024 = 1{,}048{,}576$; and the FFT requires complex multiplications $N/2 \log_2 N$ that come down to $(1024/2) \times \log(2^{1024}) = 5120$.

7.4. Numerical example

Implementation of the algorithm is described with the typical example:

$h[n] = \{1,\ 3,\ -1,\ -2\}$ and $x[n] = \{1,\ 2,\ 0,\ -1\}$.

The output is the product of the two sets:

$$Y(0) = X(0).H(0) = 2$$
$$Y(1) = X(1).H(1) = -13 - j11$$
$$Y(2) = X(2).H(2) = 0$$
$$Y(3) = X(3).H(3) = -13 + j11$$

The IDFT would yield the output in discrete time domain:

$$Y(0) = \tfrac{1}{4}[Y(0) + Y(1) + Y(2) + Y(3)] = -6$$
$$Y(1) = \tfrac{1}{4}[Y(0) + Y(1)e^{j\frac{\pi}{2}} + Y(2)e^{j2\pi} + Y(3)e^{j\frac{3\pi}{2}}] = 7$$
$$Y(2) = \tfrac{1}{4}[Y(0) + Y(1)e^{j\pi} + Y(2)e^{j\pi} + Y(3)e^{j\frac{3\pi}{2}}] = 6$$
$$Y(3) = \tfrac{1}{4}[Y(0) + Y(1)e^{j\frac{3\pi}{2}} + Y(2)e^{j3\pi} + Y(3)e^{j\frac{9\pi}{2}}] = -5.$$

The system and signal sequences: $h[n] = \{1,\ 3,\ -1,\ -2\}$ and $x[n] = \{1,\ 2,\ 0,\ -1\}$ have a common period of 4 samples. To see that the output sequence $y[n]$ are again 4 samples long in the interval [0–3] and repeating itself, the circular convolution is verified and shown in Table 2 and utilised in Eqs. (9) and (14).

The last row of the table is identical to the answer obtained with circular convolution Eqs. (9) and (14). The filtering process considerably reduces computing time since the same values of W_N^{nk} were computed and convolved many times as the computation proceeds; where n is the sample number from $n = 0$ to $N-1$ and index k ranges over N values.

7.5. Threshold load prediction utilising convolution algorithms

7.5.1. 16-Ply panel impacted with round nose impactor

The drop-weight impact test generated data obtained for 16-Ply laminates at velocity: 3.6 and 3.7 m/s were filtered using fast Fourier algorithms (convolution based) and extrapolated to correlate to load drop in the curve indicating load threshold. It can be seen from the curves that drops occur approximately around 16 kN around 1.4 mm deflection for both the cases. Comparison of the curves in Fig. 20a and b shows that filtering process had raised the peak load quantities from 16 to 18 kN. Moreover, load drops occur at peak load (threshold) indicating matrix cracking

Table 2
Circular convolution of two sequences.

N	0	1	2	3
$x[n]$	1	2	0	−1
$x[n-1]$	−1	1	2	0
$x[n-2]$	0	−1	1	2
$x[n-3]$	2	0	−1	1
$h[0] \times [n]$	1	2	0	−1
$h[1] \times [n-1]$	−3	3	6	0
$h[2] \times [n-2]$	0	1	−1	−2
$h[3] \times [n-3]$	−4	0	2	−2
Yc$[n]$	−6	7	6	−5

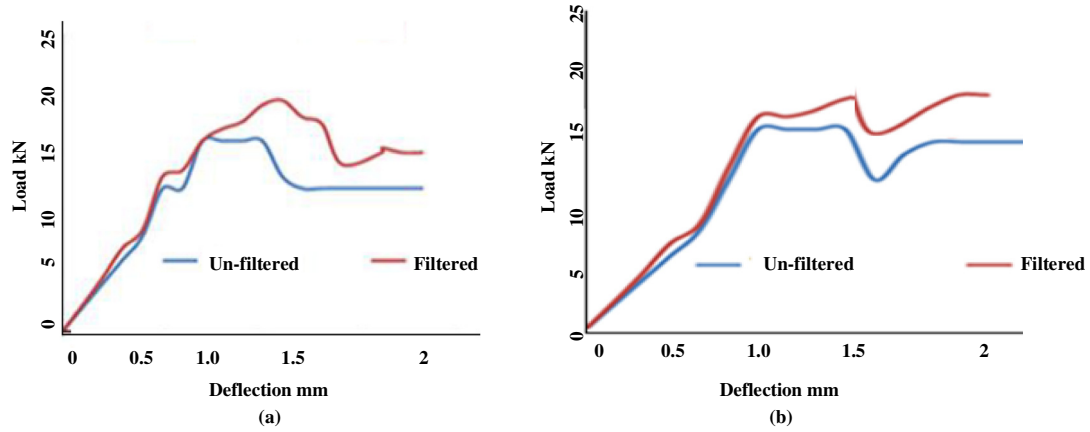

Fig. 20. Filtered load–deflection plot of 16-Ply versus flat and round nose impact.

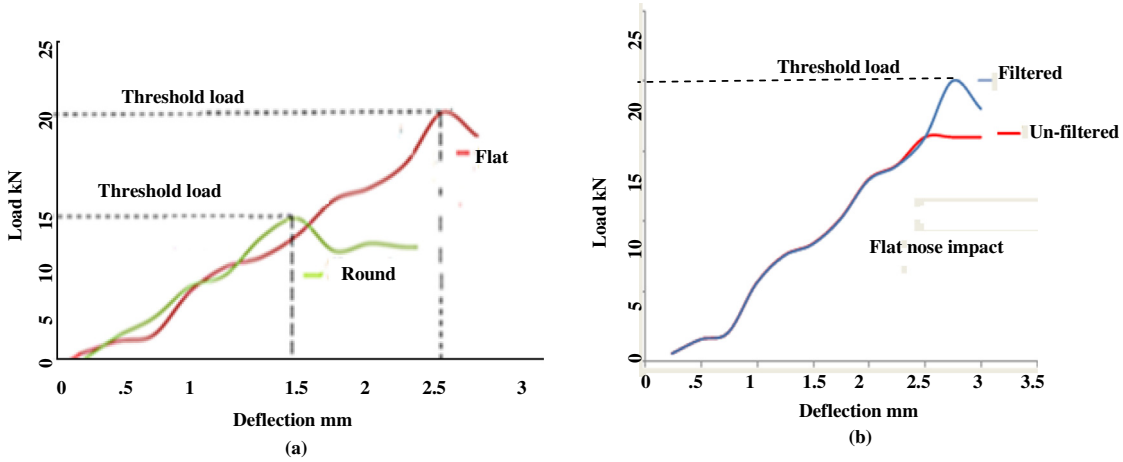

Fig. 21. Filtered load–deflection plot of 16-Ply under flat and round nose impact.

failure. No significant straight line portions of curves depicting clipped data can be seen. The results suggest that the threshold could be predicted without resorting to advanced filtering algorithms for these types of impacts.

7.5.2. Panels of different thickness versus impactor nose profiles

Another set of data obtained for 16-Ply panels impacted at velocities 3.8 m/s were filtered using fast Fourier algorithms (convolution based) and extrapolated to correlate to predict load threshold. It can be seen from the curves that drops occur approximately around 15 kN around 1.5 mm deflection for round nose impactor and load drop occurs at 20 kN under flat nose impact at 2.5 mm deflection in Fig. 21a. The data filtering algorithm successfully predicted threshold load as expected for the relatively thin panel.

Separate tests were conducted of relatively thick 24-Ply panels impacted at 4 m/s velocity with flat nose impactor. Load–deflection curves for un-filtered data show straight line of clipped data after around 18 kN as shown in Fig. 21b. Data were filtered utilising the convolution algorithm, the curve representing the filtered data raised the load level up to 22 kN where a load drop occurred. The straight line portion of the curve depicting clipped data was filtered and extrapolated to predict quantity of threshold (failure at peak load). The predicted threshold value agrees well when compared with the results obtained from non-destructive techniques Fig. 7.

7.5.3. Relatively thick 24-Ply panel impacted with flat nose impactor

The same filtering and extrapolating process was applied to the data obtained from impacts of relatively thick 24-Ply panels at 3.74 and 4.2 m/s velocities impacted with flat nose impactors. Plots of the filtered and un-filtered data are shown in Fig. 22. It can be seen that the load level increased from19 to 23 kN with velocity 3.74 m/s where expected load drop occurred Fig. 22a. The plot of impact with 4.2 m/s velocity shows increase in the load level from 20 to 24 kN and where load drop occurred (peak load as the threshold load) Fig. 22b. Comparisons of the results confirmed that the threshold load can be predicted from clipped data obtained from impact events using time-domain convolution filters and FFT algorithms.

8. Conclusions

Physical tests analogous to actual impact event of real carbon composite panels were conducted to create damage and data. Non-destructive inspections of the impacted specimens and data analysis of the test generated were performed to interpret the impact-induced damage. The data were filtered to interpret damage characteristics by comparing with damage parameters, and

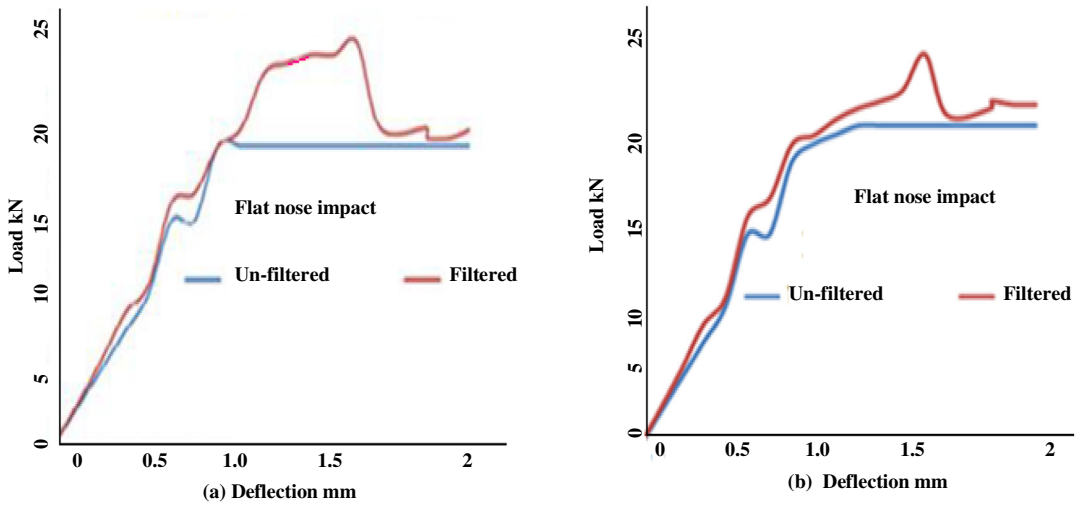

Fig. 22. Load–deflection of 24-Ply panels impacted with flat nose impactors.

to correlate and predict threshold load (where severe damage initiates) from load drops in the plots. Due to limitations of testing machine and data logging system the recorded data from flat nose impacts of twenty-four laminates were clipped that corrupted load–time plots, the expected load-drops that link damage to the load did not appear. Hence, advance data filtering and extrapolation techniques based on Fast Fourier Transforms Convolution algorithms were utilised that successfully predicted the load threshold. The following conclusions could be drawn from the observations and comparisons of the results:

- Selected laminates were C-scanned to identify damage and quantify damage zone ratios (%). The load quantities were plotted against the development sequence of the damage ratios by C-scan experiments. Comparison and correlation of the damage ratios to the FFT filtered load inflicted up to the threshold have been observed in a nearly linear relationship.
- The built-in filters were used to de-noise data produced from the impact of 8-Ply laminates and to predict threshold load.
- Statistical and numerical filters were used to filter impact induced data from 16-Ply laminate impacts to predict threshold loads up to acceptable levels.
- Advance oscillatory data filtering and extrapolation techniques based on Fast Fourier Transforms Convolution algorithms were utilised that successfully predicted the load threshold from clipped data.
- The expected linear relation was utilised to evaluate the impact-induced threshold load and estimate damage evolution in impacted panels.

Based on the results it is proposed that use of advanced data filters can enhance data interpretation and make the investigation more efficient and reliable. The proposed methodology could be useful for efficient and reliable data analysis and impact-induced damage prediction of similar case data.

References

[1] James RA. Impact damage resistance and damage tolerance of fibre reinforced laminated composites [Ph.D. thesis]. United Kingdom: University of Bolton; 2006.
[2] Hosseinzadeh R, Shokireh MM, Lessard L. Damage behaviour of fibre reinforced composite plates subjected to drop weight impacts. Compos Sci Technol 2005;66:61–8.
[3] Mitrevski T, Marshall IH, Thomson RS, Jones R. Low-velocity impacts on preloaded GFRP laminates with various impactor shapes. Compos Struct 2006;76:209–17.
[4] Kumar S, Nageswara B, Pradhan B. Effect of impactor parameters and laminate characteristics on impact response and damage in curved composite laminates. J Reinforced Plastics Compos 2007;26(13):1273–90.
[5] Ercan S, Benjamin L, Feridun D. Drop-weight impact response of hybrid composites impacted by impactor of various geometries. Mater Des 2013;52:67–77.
[6] Deng Y, Zhang W, Cao Z. Experimental investigation on the ballistic resistance of monolithic and multi-layered plates against hemispherical-nosed projectiles impact. Mater Des 2012;41:266–81.
[7] Lopes CS. Low-velocity impact damage on dispersed stacking sequence laminates. Part I. Experiments. Compos Sci Technol 2009;69(7–8):926–36.
[8] Farooq U, Peter Myler P. Finite element simulation of buckling-induced failure of carbon fibre-reinforced laminated composite panels embedded with damage zones. Acta Astronaut 2015;115:314–29.
[9] Kas YO, Kaynak C. Ultrasonic C-scan and microscopic evaluation of resin transfer moulded epoxy composite plates. Polym Testing 2004;24:114–20.
[10] Farooq U, Myler P. Flat nose low velocity drop-weight impact response of carbon fibre composites using non-destructive damage detection. De Gruyter Open Eng 2015;5:131–47.
[11] Polimeno U, Michele M, Almond DP, Angioni SL. Detecting low velocity impact damage in composite plate using nonlinear acoustic/ultrasound methods. Appl Compos Mater 2010;17:481–8.
[12] Mook G, Lange R, Koeser O. Non-destructive characterisation of carbon-fibre-reinforced plastics by means of Eddy-currents. Compos Sci Technol 2001;61:865–73.
[13] Della CN, Shu D. Vibration of delaminated composite laminates: a review. Appl Mech Rev 2007;60:1–2.
[14] Kessler SS. Damage detection in composite materials using frequency response methods. Compos Part B 2002;33(1):87–95.
[15] Farooq U, Peter Myler P. Ply level failure prediction of carbon fibre reinforced laminated composite panels subjected to low velocity drop-weight impact using adaptive meshing techniques. Acta Astronaut 2014;102:169–77.
[16] Todoroki A, Tanaka M, Yoshinobu S. Multi-prove electric potential change method for delamination monitoring of graphite/composite plates using normalized response surfaces. Compos Sci Technol 2004;62:749–58.
[17] Hoshikawa H, Koyama K. A new Eddy-current probe with minimal liftoff noise and phase information on discontinuity depth. Mater Eval 2003;61(3):423–7.
[18] Farooq U, Myler P. Efficient computational modelling of carbon fibre reinforced laminated composite panels subjected to low velocity drop-weight impact. Mater Des 2014;54:43–56.
[19] Mariani S, Corigliano A. Impact induced composite delamination: state and parameter identification via joint and dual extended Kalman filters. Comput Method Appl Mech Eng 2005;194:5242–72.
[20] Mariani S, Ghisi A. Unscented Kalman filtering for nonlinear structural dynamics. Nonlinear Dyn 2007;49:131–50.
[21] Mariani S. Failure assessment of layered composites subject to impact loading: a finite element, sigma-point Kalman filter approach failure assessment approach. Algorithms 2009;2:808–27.
[22] Julier S, Uhlmann J, Durrant-Whyte H. A new method for the nonlinear transformation of means and co-variances in filters and estimators. IEEE Trans Automat Control 2000;45:477–82.

[23] Ott Lyman R, Michael L. An introduction to statistical methods and data analysis. 6th ed. Brooks/Cole, Cengage Learning; 2008.
[24] Jie W, Fred KC, Zhenhai X. Wavelet de-noising in electrical resistance based damage detection of carbon fibre composite materials. J Mater Sci Res 2013;2(1):82–100.
[25] Yan YJ, Yam LH. Online detection of crack damage in composite plates using embedded piezoelectric actuators/sensors and wavelets analysis. Comput Struct 2002;58(1):29–38.
[26] Farooq U. Finite element simulation of flat nose low velocity impact behaviour of carbon fibre composite laminates [Ph.D. thesis]. United Kingdom: University of Bolton; 2014.